Photoredox Catalysis Mediated by Tungsten(0) Arylisocyanides

Javier Fajardo Jr., Alexandra T. Barth, Maryann Morales, Michael K. Takase, Jay R. Winkler,* and Harry B. Gray*

Beckman Institute, California Institute of Technology, Pasadena, California 91125, United States

ABSTRACT: $W(CNAr)_6$ (CNAr = arylisocyanide) photoreductants catalyze base-promoted homolytic aromatic substitution (BHAS) of 1-(2-iodobenzyl)-pyrrole in deuterated benzene. Moderate to high efficiencies correlate with $W(CNAr)_6$ excited-state reduction potentials upon one-photon 445-nm excitation, with 10 mol % loading of the most powerful photoreductants $W(CNDipp)_6$ (CNDipp = 2,6-diisopropylphenylisocyanide) and $W(CNDippPh^{OMe3})_6$ ($CNDippPh^{OMe3}$ = 4-(3,4,5-trimethoxyphenyl)-2,6-diisopropylphenylisocyanide) affording nearly complete conversion. Stern-Volmer quenching experiments indicated that catalysis is triggered by substrate reductive dehalogenation. Taking advantage of the large two-photon absorption (TPA) cross sections of $W(CNAr)_6$ complexes, we found that photocatalysis can be driven with femtosecond-pulsed 810-nm excitation. For both one- and two-photon excitation, photocatalysis was terminated by the formation of seven-coordinate W^{II}-diiodo $[WI_2(CNAr)_5]$ complexes. Notably, we discovered that $W(CNDipp)_6$ can be regenerated by chemical reduction of $WI_2(CNDipp)_5$ with excess ligand present in solution.

INTRODUCTION

Owing in part to low reorganization energies for electron transfers from relatively long-lived metal-to-ligand charge transfer (MLCT) excited states, Ru^{II} polypyridines, cyclometalated Ir^{III} 2-phenylpyridines (ppy), and their derivatives have been widely employed in photoredox catalytic cycles.[1–3] Complexes of earth-abundant metals, most notably Cu^{I} α-diimines/phosphines,[4] Zr^{IV} bis(pyrrolyl)pyridines,[5] Ce^{III} guanidinate(s)-amide(s),[6] and W^{VI} Schiff base dioxos,[7] also have shown great promise as redox photosensitizers.

In work over many years, we have demonstrated that homoleptic tungsten(0) arylisocyanides (Figure 1) are stronger photoreductants than the aforementioned Ru^{II} and Ir^{III} complexes; and, notably, $W(CNAr)_6$ complexes possess intense visible absorptions ($\varepsilon_{\lambda,max} \sim 10^4$–$10^5$ M^{-1} cm^{-1}) attributable to transitions to MLCT excited states with $E°$ ($W^+/{*}W^0$) = –2.2 to –3.0 V vs $Fc^{[+/0]}$ (* denotes the lowest energy MLCT excited state; Fc = ferrocene).[8–12] With microsecond lifetimes (τ) and large photoluminescence quantum yields (ϕ_{PL}), these $*W(CNAr)_6$ reagents efficiently reduce thermodynamically challenging substrates, including anthracene[9] and acetophenone.[10]

Of direct relevance to our work, Wenger and co-workers have investigated Cr^0 and Mo^0 tris(diisocyanides) $M(CN^RAr_3NC)_3$ (R = Me, ^{t}Bu; Figure 1); these complexes have remarkably robust, long-lived excited states with formal potentials [$E°$ ($Cr^+/{*}Cr^0$) = –2.43 V vs $Fc^{[+/0]}$ and $E°$ ($Mo^+/{*}Mo^0$) ≈ –2.6 V vs $Fc^{[+/0]}$] more negative than that of *fac*-$*Ir(ppy)_3$ ($E°$ ($Ir^{4+}/{*}Ir^{3+}$) = –2.1 V vs $Fc^{[+/0]}$).[13–15] Notably, $Mo(CN^RAr_3NC)_3$ complexes photocatalyze the rearrangement of acyl cyclopropanes to 2,3-dihydrofurans (R = Me) as well as intramolecular base-promoted homolytic aromatic substitution (BHAS) of aryl iodides (R = ^{t}Bu), reactions that are out of the potential range of *fac*-$*Ir(ppy)_3$. It also is of interest that the photocatalytic performance of isoelectronic $[Re(CN^{Me}Ar_3NC)_3]^+$ (Figure 1) for dehalogenation of halobenzenes is similar to that of *fac*-$*Ir(ppy)_3$.[16]

In light of these findings, we decided to try our $W(CNAr)_6$ complexes as photoreductants in BHAS catalytic cycles. While $W(CNAr)_6$ and $Mo(CN^RAr_3NC)_3$ possess comparable ground- and excited-state properties (Table 1), employing monodentate arylisocyanides loomed as potentially problematic, given that seven-coordinate M^{II} arylisocyanides such as $[MX(CNPh)_6]^+$ (M = Mo, W; X = Cl, I) are products of $M(CNPh)_6$ oxidation.[17–19] Furthermore, Wenger and co-workers noted that deactivation via formation of higher coordinate complexes likely was responsible for the lower efficiencies of $Mo(CN^{Me}Ar_3NC)_3$ versus $Mo(CN^{tBu}Ar_3NC)_3$ in photoredox catalysis, with the less sterically shielded complex being more susceptible to nucleophilic attack on the Mo^I center by the iodide generated upon substrate reductive dehalogenation.[15]

That said, several observations suggested that $W(CNAr)_6$ complexes might be competent photoredox catalysts. One was that photosubstitution quantum yields (ϕ_{PS}) for CNAr displacement upon 436-nm irradiation of $W(CNAr)_6$ in neat pyridine solution decreased greatly upon increasing the ligand sterics from phenylisocyanide (Ar = Ph, ϕ_{PS} = 0.011) to 2,6-diisopropylphenylisocyanide (CNDipp, ϕ_{PS} = 0.003), indicating that associative pyridine substitution occurs in the $*W(CNAr)_6$ reaction.[17,18] Additionally, although 436-nm irradiation of $W(CNPh)_6$ in $CHCl_3$ solution afforded the W^{II} seven-coordinate product $[WCl(CNPh)_6]^+$, similar irradiation of $W(CNDipp)_6$ instead yielded the six-coordinate cation $[W(CNDipp)_6]^+$.[17,18] Taken together, these findings indicate that the use of bulky 2,6-isopropyl-substituted monodentate arylisocyanides likely would provide enough steric protection to enable efficient BHAS photocatalysis.

In prior work we demonstrated that three $W(CNAr)_6$ photoreductants exhibit extremely large two-photon absorption (TPA) cross sections ($\delta > 10^3$ GM).[20] In the context of photoredox catalysis, near-infrared (NIR) two-photon excitation can be used to generate reactive $W(CNAr)_6$ MLCT excited states without competitive absorption or photoreactivity by the substrate. Also of great interest is the emerging technology of two-photon

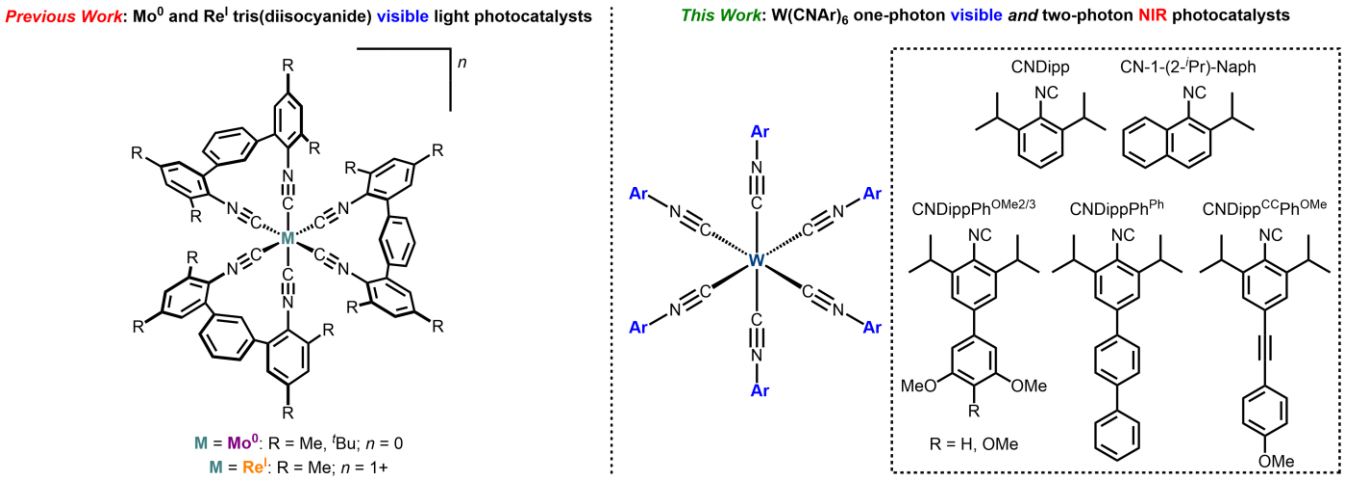

Figure 1. $[M(CN^{R}Ar_3NC)_3]_n$ (refs. 15,16) and $W(CNAr)_6$ homoleptic arylisocyanide photocatalysts.

photochemistry in nano- to microscale 3D printing, wherein multiphoton-triggered free-radical polymerization creates cross-linked polymeric materials with extremely high spatial resolution (< 100 nm). [21] However, a current challenge for the advancement of this field is discovery of new photointiators with large TPA cross-sections.[21a] Herein, we report large δ values for eight additional $W(CNAr)_6$ photoreductants and demonstrate their capacity to generate organic radicals upon two-photon ultrafast laser excitation. Of note, $W(CNAr)_6$ complexes are capable of driving both one-photon visible and two-photon NIR BHAS photoredox catalysis.

RESULTS AND DISCUSSION

$W(CNAr)_6$ One-Photon Photoredox Catalysis. In addition to the parent complex, $W(CNDipp)_6$, five representative photoreductants from two subsequent generations of $W(CNAr)_6$ compounds were investigated. From the oligoarylisocyanide series, we elected to explore $W(CNDippPh^{OMe2})_6$ and $W(CNDippPh^{OMe3})_6$, as the methoxy substituents impart greater solubility in a variety of solvents. We also studied $W(CNDippPh^{Ph})_6$ to see how a more radially extended aromatic system affects reactivity. And finally, we included $W(CNDipp^{CC}Ph^{OMe})_6$ and W(CN-1-(2-^{i}Pr)-Naph)$_6$ in our investigation, as they are very strong photoreductants with among the longest excited-state lifetimes of all $W(CNAr)_6$ complexes. Relevant properties of the $W(CNAr)_6$ photocatalysts are set out in Table 1.

Previously reported ground-state electrochemical data for all $W(CNAr)_6$ complexes in this study were collected under slightly different conditions. For consistency in comparisons of ground-state $W^{[+/0]}$ and excited-state $W^{+}/{*}W^{0}$ formal potentials, we acquired cyclic voltammograms (CVs) for $W(CNDipp)_6$, $W(CNDippPh^{OMe3})_6$, and $W(CNDippPh^{Ph})_6$ under conditions analogous to those for $W(CNDipp^{CC}Ph^{OMe})_6$ and W(CN-1-(2-^{i}Pr)-Naph)$_6$ (Supporting Information). The full CVs of these complexes are typical of $W(CNAr)_6$ compounds,[12,19,22] with reversible $W^{[+/0]}$ couples exhibiting scan-rate dependences indicating diffusion-controlled processes (Figures S138–S144). The revised ground-state and excited-state formal potentials are in Table 1. Because $E°$ ($W^{[+/0]}$) values range from –0.42 to –0.56 V vs $Fc^{[+/0]}$, strong sacrificial reductants would be needed for regeneration of $W(CNAr)_6$ in some photocatalytic cycles. For that reason, we chose to explore BHAS organic reactions, as they simplify photoredox cycles by obviating the need for sacrificial reductants.

As a starting point, we examined the intramolecular photoreaction of BHAS substrate 1-(2-iodobenzyl)-pyrrole (50 mM) in the presence of ca. 5 mol % $W(CNAr)_6$ and 2 equivalents (equiv) of 2,2,6,6-tetramethylpiperidine (TMP) in C_6D_6 (Table 2). Under similar conditions, $Mo(CN^{R}Ar_3NC)_3$ efficiently catalyzed the reaction upon irradiation at 470 nm (14 W) for 1 h (Table 2, entry 12).[15] Compared to this benchmark, 445-nm irradiation (6 W) of the parent complex $W(CNDipp)_6$ for 1 h afforded 62% conversion to the cyclized product (by ^{1}H NMR spectroscopy; Table 2, entry 2). This conversion corresponds to a turnover number (TON) of 11, demonstrating that $W(CNDipp)_6$ is a photocatalyst for the BHAS reaction. A colorless crystalline solid, identified as 2,2,6,6-tetramethylpiperidinium iodide [H–TMP][I], precipitated from solution within seconds of commencing irradiation. After 1-h irradiation, $W(CNDipp)_6$ was no longer present in the reaction mixture, as confirmed by ^{1}H NMR and UV–visible spectroscopic data. Accordingly, sample luminescence and further conversion were not observed at longer irradiation times (Figure 2). Instead, free

Table 1. Properties of $W(CNAr)_6$ and $Mo(CN^{tBu}Ar_3NC)_3$ Photocatalysts[a]

Photocatalyst	λ_{max}[e]	$\varepsilon_{\lambda,max}$[f]	λ_{exc}[e]	$\varepsilon_{\lambda,exc}$[f]	τ[g]	ϕ_{PL}	$E°$ ($W^{[+/0]}$)[h]	$E°$ ($W^{+}/{*}W^{0}$)[h]
$W(CNDipp)_6$[b]	465	9.5 x 10^4	445	8.0 x 10^4	0.12	0.03	–0.56	–2.84
$W(CNDippPh^{OMe3})_6$[b]	495	1.3 x 10^5	445	6.7 x 10^4	1.83	0.41	–0.53	–2.68
$W(CNDippPh^{Ph})_6$[b]	506	1.6 x 10^5	445	7.5 x 10^4	1.53	0.44	–0.52	–2.60
W(CN-1-(2-^{i}Pr)-Naph)$_6$[c]	509	5.7 x 10^4	445	4.6 x 10^4	3.83	0.25	–0.47	–2.49
$W(CNDipp^{CC}Ph^{OMe})_6$[c]	518	1.6 x 10^5	445	5.7 x 10^4	1.82	0.78	–0.42	–2.43
$Mo(CN^{tBu}Ar_3NC)_3$[d]	400	3.0 x 10^4	470	2.7 x 10^4	1.29	0.20	–0.46	–2.7

[a]Collected from deaerated room temperature toluene solutions. [b]Data from ref. 10. [c]Data from ref. 12. [d]Data from ref. 15 (λ_{max}, $\varepsilon_{\lambda,max}$, and $\varepsilon_{\lambda,exc}$ were estimated from the plot in Figure 2 of this reference; τ is the weighted average lifetime). [e]nm. [f]M^{-1} cm^{-1}. [g]μs. [h]V vs $Fc^{[+/0]}$. Ground-state electrochemical measurements performed in tetrahydrofuran (THF) with 0.1 M [^{n}Bu$_4$N][PF_6] supporting electrolyte.

Table 2. One-Photon Photoredox Catalysis Mediated by W(CNAr)$_6$ Complexes[a]

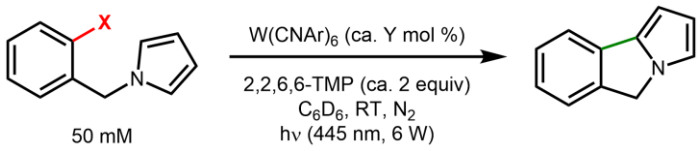

Entry	W(CNAr)$_6$	X	Y	Irrad Time (h)	Conversion (%)[b]	TON
1	W(CNDipp)$_6$	I	2.5	1	28	11
2	W(CNDipp)$_6$	I	5	1	62	11
3	W(CNDipp)$_6$	I	10	4	98	8
4	W(CNDipp)$_6$	Br	10	12	14	1
5	W(CNDippPh^{OMe3})$_6$	I	2.5	1	42	15
6	W(CNDippPh^{OMe3})$_6$	I	5	4	85	16
7	W(CNDippPh^{OMe3})$_6$	I	10	4	98	9
8	W(CNDippPh^{OMe2})$_6$	I	5	4	88	17
9	W(CNDippPh^{Ph})$_6$	I	5	12	84	15
10	W(CN-1-(2-*i*Pr)-Naph)$_6$	I	5	12	42	7
11	W(CNDipp^{CC}Ph^{OMe})$_6$	I	5	12	24	4
12	Mo(CN$^{t\text{Bu}}$Ar$_3$NC)$_3$[d]	I	5	1	100	20
13	*fac*-Ir(ppy)$_3$[d,e]	I	5	1	4	1
14	W(CNAr)$_6$	I	5	*c*	0	0
15	None	I	0	4	0	0

[a]Reactions performed in J-Young NMR tubes. Irradiation with a high-power blue diode laser. Reported results are from single run experiments. See Supporting Information for precise reagent stoichiometries. [b]Substrate conversion calculated by relative integration of the ^{1}H NMR benzylic resonances of the product and starting material. [c]Sample stored in the dark at room temperature (RT) for 4 h. [d]Data from ref. 15. Irradiation with a 470 nm LED operating at 14 W. [e]Similar conversion observed when irradiated at 405 nm instead of 470 nm.

CNDipp and a new set of isopropyl resonances corresponding to a diamagnetic deactivation product (*vide infra*) appeared in the ^{1}H NMR spectrum.[23]

We next explored the photoredox activities of second and third generation W(CNAr)$_6$ complexes. Interestingly, despite being a slightly weaker photoreductant, W(CNDippPh^{OMe3})$_6$ was able to drive the BHAS reaction to 85% completion (TON = 16) after 4-h irradiation (Table 2, entry 6). We found that W(CNDippPh^{OMe2})$_6$, which has virtually identical ground- and excited-state properties as W(CNDippPh^{OMe3})$_6$,[10] catalyzed the reaction with similar efficiency (Table 2, entry 8). As occurs during W(CNDipp)$_6$ photocatalysis, [H–TMP][I] precipitated upon progression of the reaction, W(CNDippPh$^{OMe2/3}$)$_6$ complexes were no longer present after 4-h irradiation, and deactivation products appeared (isopropyl resonances attributable to such products were observed in the ^{1}H NMR spectrum).

In contrast to biarylisocyanide photocatalysis, 445-nm irradiation of a BHAS reaction containing ca. 5 mol % W(CNDippPh^{Ph})$_6$ for 4 h only reached 53% conversion (TON = 9; Figure 2). However, after 12-h irradiation, conversion to product was about the same as that for W(CNDippPh$^{OMe2/3}$)$_6$ (Figure 2; Table 2, entry 9). Following this trend, reactions with photoreductants W(CN-1-(2-*i*Pr)-Naph)$_6$ and W(CNDipp^{CC}Ph^{OMe})$_6$ reached 28% (TON = 5) and 13% (TON = 2) conversion after 4-h irradiation (Figure 2); the yields increased to 42% (TON = 7; Table 2, entry 10) and 24% (TON = 4; entry 11) after 12 h. Importantly, W(CNDippPh^{Ph})$_6$, W(CN-1-(2-*i*Pr)-Naph)$_6$, and W(CNDipp^{CC}Ph^{OMe})$_6$ were still present at the 12-h irradiation point (as determined by ^{1}H NMR, UV–vis, and the luminescence of photoredox samples), suggesting that photocatalyst

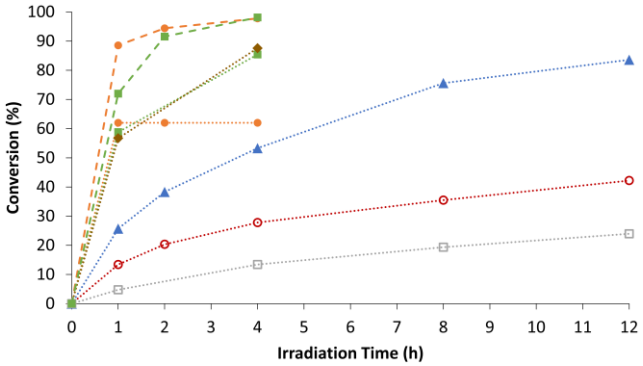

Figure 2. Time profiles of the BHAS photoredox reaction catalyzed by W(CNAr)$_6$ employing one-photon 445-nm excitation. Dotted and dashed lines, which are provided as guides for the eye only, represent ca. 5 and 10 mol % W(CNAr)$_6$ photocatalyst loading, respectively. Color/marker code: W(CNDipp)$_6$ (orange; solid circle), W(CNDippPh^{OMe3})$_6$ (green; solid square), W(CNDippPh^{OMe2})$_6$ (brown; diamond), W(CNDippPh^{Ph})$_6$ (blue; triangle), W(CN-1-(2-*i*Pr)-Naph)$_6$ (red; open circle), W(CNDipp^{CC}Ph^{OMe})$_6$ (gray; open square).

decomposition did not limit conversion.

Although their efficiencies were somewhat lower than that for Mo(CN$^{t\text{Bu}}$Ar$_3$NC)$_3$ at a similar catalyst loading, all investigated W(CNAr)$_6$ complexes were active photoredox catalysts. Owing in part to more negative excited-state potentials, they performed better than *fac*-Ir(ppy)$_3$ (Table 2, entry 13).[15] We emphasize that monitoring substrate solutions in the absence of W(CNAr)$_6$ or light confirmed that both components were essential for photocatalysis (Table 2, entries 14 and 15).

Given the favorable results obtained with W(CNDipp)$_6$ and W(CNDippPh^{OMe3})$_6$, we investigated the effect of photocatalyst loading on reaction conversion. Decreasing the W(CNAr)$_6$ loading by half reduced the conversion by half, albeit with comparable TONs (CNDipp: Table 2, entry 1; CNDippPh^{OMe3}: entry 5).[24] Alternatively, doubling the loading to ca. 10 mol % afforded near quantitative substrate conversion (CNDipp: 98%, Table 2, entry 3; CNDippPh^{OMe3}: 98%, entry 7). Consistent with the high yield achieved with ca. 5 mol % W(CNDippPh^{OMe3})$_6$, a substantial amount of photocatalyst was present (by ^{1}H NMR spectroscopy) upon reaction termination.

Encouraged by the above results with 1-(2-iodobenzyl)-pyrrole, we turned our attention to the analogous bromo substrate, 1-(2-bromobenzyl)-pyrrole. Subjecting this substrate to photoredox catalysis conditions with ca. 10 mol % W(CNDipp)$_6$ loading yielded 14% conversion after 12-h irradiation (Table 2, entry 4). For comparison, *Mo(CN^t^{Bu}Ar$_3$NC)$_3$, a ca. 100 mV weaker photoreductant, only reached 7% conversion after 18-h irradiation.[15] These results are consistent with reductive dehalogenation by *W(CNAr)$_6$ as the initial step in the photodriven BHAS reaction (*vide infra*), as aryl bromides are more difficult to reduce than aryl iodides. Moreover, there was a substantial amount of W(CNDipp)$_6$ remaining after 12-h irradiation, indicating that performance was not limited by catalyst decomposition.

To gain further insight into the above trends among conversion efficiency, irradiation time, and $E°$ (W$^+$/*W^0), we conducted Stern-Volmer quenching experiments using W(CNDipp)$_6$, W(CNDippPh^{OMe3})$_6$, and W(CN-1-(2-^{i}Pr)-Naph)$_6$ as representative complexes. Although we previously collected photophysical and photochemical data for W(CNAr)$_6$ in toluene and THF solution, we performed Stern-Volmer experiments in benzene solution to mimic the photoredox catalysis conditions as closely as possible and minimize side reactions with intermediate aryl radicals. As the steady-state absorption and luminescence spectra of W(CNDipp)$_6$, W(CNDippPh^{OMe3})$_6$, and W(CN-1-(2-^{i}Pr)-Naph)$_6$ in benzene and toluene are nearly identical (Figures S21–S23), we anticipated the excited-state dynamics would also be very similar in the two solvents. Indeed, transient absorption (TA) spectra showed that *W(CNAr)$_6$ reagents were generated in benzene solution following excitation, and data obtained from time-resolved luminescence decays and TA bleach recoveries (*W(CNDipp)$_6$: 116 ns; *W(CNDippPh^{OMe3})$_6$: 1.76 μs; *W(CN-1-(2-^{i}Pr)-Naph)$_6$: 3.65 μs) confirmed that the lifetimes were comparable to those in toluene solution (Table 1; see Supporting Information for details).

Substrate 1-(2-iodobenzyl)-pyrrole quenched the luminescences of *W(CNDipp)$_6$, *W(CNDippPh^{OMe3})$_6$, and *W(CN-1-(2-^{i}Pr)-Naph)$_6$ with varying rate constants (k_q) 6.2 × 10^7, 1.3 × 10^7, and 2.2 × 10^6 M^{-1} s^{-1} (Table 3; Figures S133–S136). Notably, these k_q values are in line with electron-transfer driving forces ($\Delta G°_{ET}$) for reduction of the iodoarene substrate (approximated as $E°$ (Ph–I$^{[0/-]}$) ~ –2.64 V vs Fc$^{[+/0]}$ for iodobenzene;[25] Table 3). In photoreactions in solutions with 50 mM quencher, the longer lifetimes of *W(CNDippPh^{OMe3})$_6$ and *W(CN-1-(2-^{i}Pr)-Naph)$_6$ account for relatively high initial quenching yields (ϕ_q; Table 3).

We also found that 1-(2-bromobenzyl)-pyrrole quenched the luminescence of *W(CNDipp)$_6$ in benzene solution (Figure S134): k_q (8.6 x 10^6 M^{-1} s^{-1}) was nearly an order of magnitude smaller than that for 1-(2-iodobenzyl)-pyrrole, as expected for a reaction with lower driving force [*W(CNDipp)$_6$: $E°$ (W$^+$/*W^0) = –2.84 V vs Fc$^{[+/0]}$; aryl bromide substrate: approximated as $E°$ (Ph–Br$^{[0/-]}$) ~ –2.84 V vs Fc$^{[+/0]}$ for bromobenzene;[25] Table 3)]. Unsurprisingly, ϕ_q for the bromo substrate was much lower than that for 1-(2-iodobenzyl)-pyrrole (Table 3).

The W(CNAr)$_6$ version of Wenger's mechanism for Mo(CN^t^{Bu}Ar$_3$NC)$_3$-mediated BHAS photoredox catalysis is shown in Figure 3. Following 445-nm excitation of W(CNAr)$_6$, *W(CNAr)$_6$ rapidly reduced the substrate. The quenching reaction generated [W(CNAr)$_6$]$^+$ along with halide and the corresponding organic aryl radical. After intramolecular cyclization of the latter, which likely occurred very rapidly, reduction of [W(CNAr)$_6$]$^+$ by the pyrrole-based radical regenerated the starting W^0 photocatalyst. In the final step, deprotonation of the tricyclic organic cation by TMP yielded the cyclized product and [H–TMP][X], closing the productive cycle. The consumption of W(CNAr)$_6$ during turnover suggests that a decomposition reaction competed with reduction of [W(CNAr)$_6$]$^+$ by the pyrrole-based radical. Moreover, conversion efficiencies did not track

Table 3. Stern-Volmer Quenching Constants and Reaction Driving Forces[a]

W(CNAr)$_6$	Quencher	k_q[b]	ϕ_q[c]	Conversion[d]	$E°$ (Ph-X$^{[0/-]}$)[f,g]	$E°$ (W$^+$/*W^0)[f]	$\Delta G°_{ET}$[h]
W(CNDipp)$_6$	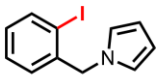	6.2 x 10^7	0.27	62%	–2.64	–2.84	–0.20
W(CNDipp)$_6$	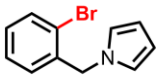	8.6 x 10^6	0.05	3%[e]	–2.84	–2.84	0
W(CNDippPh^{OMe3})$_6$	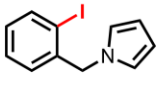	1.3 x 10^7	0.54	59%	–2.64	–2.68	–0.04
W(CN-1-(2-^{i}Pr)-Naph)$_6$	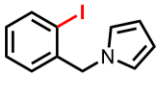	2.2 x 10^6	0.30	13%	–2.64	–2.49	+0.15

[a]Stern-Volmer quenching experiments performed in deaerated room temperature benzene solutions. [b]M^{-1} s^{-1}. [c]Initial quenching yields for a substrate concentration of 50 mM. [d]After 1-h irradiation (445 nm, 6 W) of photoredox reactions with ca. 5 mol % W(CNAr)$_6$ loading. [e]ca. 10 mol % W(CNDipp)$_6$ loading. [f]V vs Fc$^{[+/0]}$. [g]Reduction potentials for iodobenzene and bromobenzene reported in V vs SCE in ref. 25 were converted to V vs Fc$^{[+/0]}$ using the approximation $E°$ (Fc$^{[+/0]}$) = +0.4 V vs SCE. [h]eV.

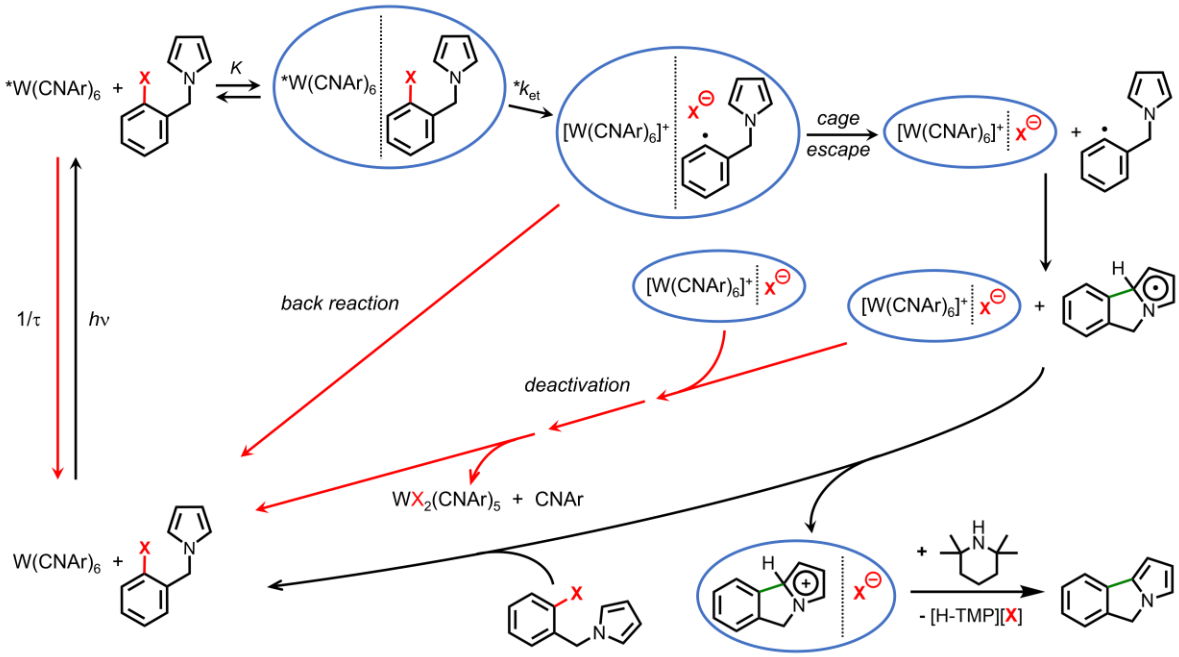

Figure 3. Proposed mechanism of BHAS photoredox catalysis in benzene solution mediated by $W(CNAr)_6$ complexes. Productive catalysis pathways are shown as black arrows; unproductive back-reaction and deactivation pathways are indicated with red arrows. Electron-transfer quenching of $*W(CNAr)_6$ involves formation of a precursor complex (equilibrium constant K) followed by concerted electron transfer and C–X bond cleavage (rate constant $*k_{et}$). The observed quenching rate constant is $k_q = K*k_{et}$. Ion-pair separation from solvent cages (blue ellipses) is unfavorable in benzene; only the neutral organic radical is likely to escape the solvent cage after quenching. Adapted in part with permission from ref. 15. Copyright 2019 American Chemical Society.

with ϕ_q, indicating that there were additional loss pathways.

Given that ground-state $W(CNAr)_6^{[+/0]}$ formal potentials range from –0.42 to –0.56 V vs $Fc^{[+/0]}$, the $\Delta G°_{ET}$ values associated with reduction of $[W(CNAr)_6]^+$ by the intermediate tricyclic organic radical also will vary, leading to different rates of $W(CNAr)_6$ regeneration, which in turn likely account for different rates of photocatalyst deactivation via nucleophilic attack of $[W(CNAr)_6]^+$ by the halide anion liberated in the reductive dehalogenation step (*vide infra*).

The BHAS reactions photocatalyzed by $W(CNAr)_6$ complexes are consistent with our amended version of Wenger's mechanism. Under a uniform set of reaction conditions (Figure 2), two differences are apparent among the $W(CNAr)_6$ complexes: (i) conversion rates tend to decrease as the $*W(CNAr)_6$ reducing power decreases; and (ii) conversion yields are highly variable. The initial 1-(2-iodobenzyl)-pyrrole quenching yields for $W(CNDipp)_6$, $W(CNDippPh^{OMe3})_6$, and $W(CN\text{-}1\text{-}(2\text{-}^i Pr)\text{-}Naph)_6$ are > 25% and bear no relationship to conversion rates. Slow conversion in the presence of efficient quenching is a hallmark of competition between back reaction and cage escape after quenching. Back reaction is unexpected since reduction of aryl iodides is believed to involve concerted electron transfer and C–I bond cleavage.[25] Of relevance here, however, is the report by Savéant that less than unit product-formation quantum yields for concerted C–X bond cleavage can occur during phototriggered reductions of aryl halide substrates.[26] Competition between back reaction and cage escape after quenching can rationalize our observation that slower conversion rates correlate with higher back-reaction driving forces (increasing $E°(W^{[+/0]})$).

Low cage-escape efficiency likely is responsible for the twenty-fold reduction in product conversion with 1-(2-bromobenzyl)-pyrrole compared to the aryl iodide. A factor of 5.5 was expected on the basis of ϕ_q. In contrast to aryl iodides, reduction of aryl chlorides and bromides is thought to proceed via a two-step mechanism with an intermediate radical anion.[25] It is likely, then, that the large reduction in product conversion with the aryl bromide substrate is due to less efficient quenching coupled with rapid back reaction between $[W(CNAr)_6]^+$ and $[Ar–Br]^{\bullet-}$ prior to radical escape from the solvent cage..

The variations in conversion efficiencies and $W(CNAr)_6$ consumption during catalysis indicate that a $[W(CNAr)_6]^+$ decomposition pathway competes with productive reaction between the cation and the intermediate aryl radical. $W(CNDipp)_6$ reaches limiting 62% conversion and full W^0 consumption after 1 h (or less) of irradiation, indicative of a high radical cage-escape yield and rapid $[W(CNDipp)_6]^+$ decomposition. Doubling the $W(CNDipp)_6$ loading leads to higher conversion because more time is required to deplete the $W(CNDipp)_6$ complex. $W(CNDippPh^{OMe3})_6$, $W(CNDippPh^{OMe2})_6$, and $W(CNDippPh^{Ph})_6$ achieve higher conversions (> 80%) than $W(CNDipp)_6$, albeit more slowly, consistent with diminished radical cage-escape yields after quenching, but more favorable competition between $[W(CNAr)_6]^+$ decomposition and reduction. Low radical cage-escape efficiency after quenching slows photocatalysis with $W(CN\text{-}1\text{-}(2\text{-}^i Pr)\text{-}Naph)_6$ and $W(CNDipp^{CC}Ph^{OMe})_6$ to the point that limiting conversion is not reached after 12 h of irradiation.

Two-Photon Photoredox Catalysis. All investigated $W(CNAr)_6$ complexes displayed photoluminescence upon femtosecond-pulsed 810-nm excitation; and $*W(CNAr)_6$ emission spectra obtained following one- or two-photon excitation were virtually identical (Figure 4), confirming that the same long-lived excited triplet (^{3}MLCT) photoreductant was generated in both cases. In 2-methyl THF solution, $W(CNDippPh^{OMe2/3})_6$ and $W(CNDippPh^{Ph})_6$ exhibited very large two-photon absorption cross sections [δ = 1000–2000 GM (1 GM = 10^{-50} cm^4 s $photon^{-1}$ $molecule^{-1}$)] upon excitation at 812 nm.[20] We have extended this work to include TPA cross sections for all three generations of $W(CNAr)_6$ complexes in toluene solution

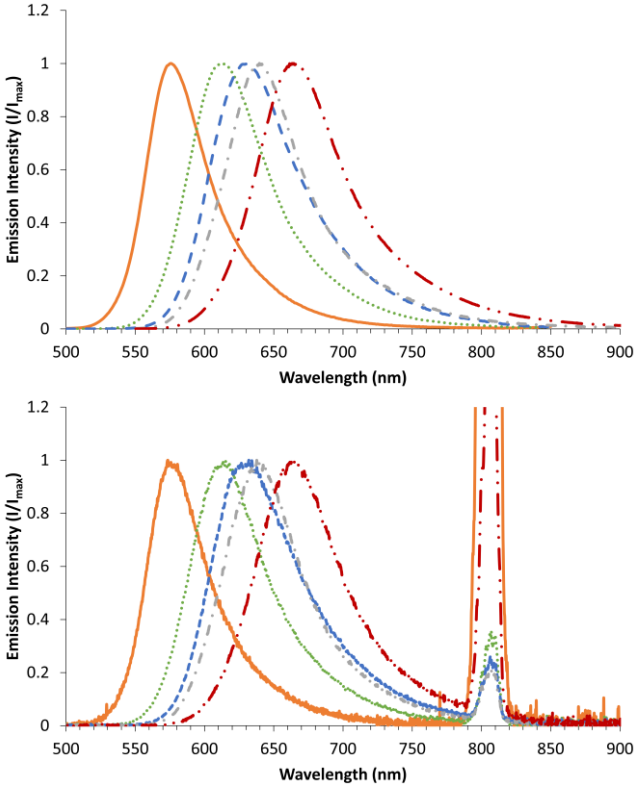

Figure 4. Stacked luminescence spectra collected upon one-photon (top) and two-photon (810 nm; bottom) excitation of W(CNDipp)$_6$ (orange; solid trace), W(CNDippPh^{OMe3})$_6$ (green; dotted trace), W(CNDippPh^{Ph})$_6$ (blue; dashed trace), W(CNDipp^{CC}Ph^{OMe})$_6$ (gray; dotted-dashed trace), and W(CN-1-(2-*i*Pr)-Naph)$_6$ (red; double dotted-dashed trace) in room temperature toluene solution. For the bottom spectra, the signal at 810 nm corresponds to scattered excitation light from the femtosecond-pulsed Ti:Sapphire laser.

(810-nm excitation; Table 4). As δ values for $[Ru(bpy)_3]^{2+}$ (bpy = 2,2'-bipyridine; δ_{812} = 7 GM)[20] and *fac*-Ir(ppy)$_3$ (δ_{800} = 20 GM)[27] are orders of magnitude smaller at similar wavelengths, our scalable tungsten complexes have the potential to displace ruthenium and iridium photosensitizers in two-photon biological imaging, photodynamic therapy, and photoredox catalysis applications (*vide infra*).

Table 4. Two-Photon Absorption (TPA) Cross Sections of W(CNAr)$_6$ Complexes[a]

W(CNAr)$_6$	δ_{810} (GM)
W(CNDipp)$_6$	230 ± 14
W(CNDippPh)$_6$	1000 ± 220
W(CNDippPh^{OMe2})$_6$	1100 ± 130
W(CNDippPh^{OMe3})$_6$	970 ± 96
W(CNDippPh^{Ph})$_6$	1900 ± 280
W(CNDipp^{CC}Ph^{OMe})$_6$	1100 ± 70
W(CNDipp^{CC}Ph)$_6$	1100 ± 160
W(CNDipp^{CC}-1-Naph)$_6$	1100 ± 180
W(CNDipp^{CC}-9-Phen)$_6$	1100 ± 160
W(CNDipp^{CC}Ph^{CN})$_6$	480 ± 50
W(CN-1-(2-*i*Pr)-Naph)$_6$	180 ± 40

[a]Collected from complexes in deaerated room temperature toluene solution: fs-pulsed 810-nm excitation (Ti:Sapphire laser); the δ_{810} values are an average of three measurements.

In our exploration of two-photon BHAS photocatalysis, we employed conditions that were optimal for one-photon reactions, namely ca. 10 mol % loading of W(CNDipp)$_6$ or W(CNDippPh^{OMe3})$_6$. We found that both complexes catalyzed BHAS of 1-(2-iodobenzyl)-pyrrole upon fs-pulsed 810-nm irradiation, with 56% (TON = 5) and 33% (TON = 3) conversion observed for W(CNDipp)$_6$ and W(CNDippPh^{OMe3})$_6$ after 12-h irradiation in C_6D_6 solution, respectively (Table 5). Owing to differences in laser power and two-photon cross sections, the W(CNDippPh^{OMe3})$_6$ excitation rate was 1.7 times that for W(CNDipp)$_6$. The higher W(CNDipp)$_6$ conversion efficiency with a nearly two-fold lower excitation rate is consistent with a lower cage-escape yield for W(CNDippPh^{OMe3})$_6$.

Table 5. Two-Photon NIR Photoredox Catalysis Mediated by W(CNDipp)$_6$ and W(CNDippPh^{OMe3})$_6$ Complexes[a]

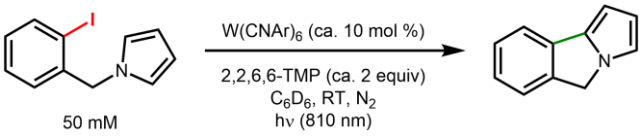

W(CNAr)$_6$	Irrad Time (h)	Conversion (%)[b]	TON
W(CNDipp)$_6$	12	56	5
W(CNDippPh^{OMe3})$_6$	12	33	3

[a]Irradiation with a fs-pulsed Ti:Sapphire laser. [b]Substrate conversion calculated by relative integration of the ^{1}H NMR benzylic resonances of the product and starting material.

In related work, Rovis and co-workers reported that Os^{II} polypyridines function as NIR photoredox catalysts.[28,29] Interestingly, the reactive Os^{II} MLCT states can be generated via one-photon $S_0 \rightarrow T_1$ NIR excitation. It also is worth noting that photoredox[30] and photoisomerization[31] reactions can be triggered by triplet fusion NIR-to-visible upconversion.

WI$_2$(CNAr)$_5$ Deactivation Products. We observed that W(CNAr)$_6$ complexes were consumed during catalytic photoredox reactions involving haloaryl substrates. Concomitantly, new sets of diamagnetic isopropyl resonances appeared in ^{1}H NMR spectra. While one set of resonances was assignable to uncomplexed CNAr, we suspected that the other set belonged to an uncharged, C_6D_6-soluble tungsten complex. We therefore set out to synthesize and characterize one or more deactivation products and establish whether such species could re-enter photocatalytic cycles.

On pursuing the aforementioned products, we found that stoichiometric photoreduction of iodobenzene by *W(CNDipp)$_6$ in room temperature benzene solution proceeded over the course of several hours with loss of sample luminescence to yield a new diamagnetic tungsten arylisocyanide complex (Scheme 1). Of relevance is that the UV–vis and ^{1}H NMR spectra of this new compound matched those acquired at the termination of W(CNDipp)$_6$-mediated photoredox catalysis (Figures S47–S49). Following crystallization by slow evaporation of a concentrated benzene solution, seven-coordinate WI$_2$(CNDipp)$_5$ was isolated in 95% yield (XRD structure; Figure 5).

The geometry of WI$_2$(CNDipp)$_5$ in the solid state approximates a capped octahedron, where one CNDipp serves as the capping ligand to the tris(CNDipp) face, and the uncapped face is occupied by the remaining CNDipp and two iodide ligands. In this regard, its structure is analogous to that of WI$_2$(CO)(CN^{t}Bu)$_4$,[32] wherein the carbonyl ligand caps the

Scheme 1. Synthesis of $WI_2(CNAr)_5$ Complexes

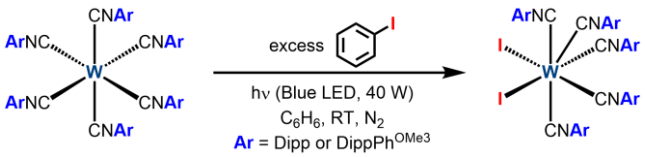

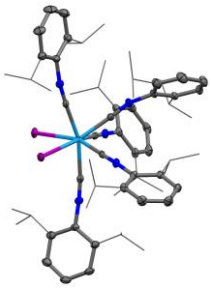

Figure 5. Structure of crystalline $WI_2(CNDipp)_5$ with thermal ellipsoids set at 50% probability. Isopropyl groups are presented as wireframes and hydrogen atoms omitted for clarity. Atom color code: W, teal; I, purple; N, blue; C, gray.

tris(CN^{t}Bu) face of the octahedron. Interestingly, as in $WI_2(CO)(CN^tBu)_4$, the weakly bound isocyanide (based on its relatively long W–C bond) in $WI_2(CNDipp)_5$ resides in the uncapped face. It is worth noting that while the related compounds $MoX_2(CN\text{-}p\text{-tolyl})_5$ (X = Cl, Br) have been reported,[33] complexes of the composition $MX_2(CNR)_5$ (M = Mo, W; X = halide; R = alkyl or aryl) have seldom been spectroscopically or structurally characterized.[34] Seven-coordinate M^{II} (M = Mo, W) homoleptic isocyanides $[M(CNR)_7][X]_2$,[19,35] mixed halide-isocyanides $[MX(CNR)_6][X]$,[19,35[c,h],36] and mixed halide-isocyanide-carbonyls $MX_2(CO)_{5-y}(CNR)_y$ (y = 2–4)[35h,37] are more common. The W–I and W–C bond lengths in $WI_2(CNDipp)_5$ fall within the range observed for structurally characterized coordination compounds of this latter type.

In room temperature C_6D_6 solution, $WI_2(CNDipp)_5$ displayed a single set of ^{1}H and ^{13}C NMR resonances for the CNDipp ligands, suggesting that the isocyanides exchange rapidly on the NMR timescale. Such fluxionality is typical of related seven-coordinate (halide-)isocyanide M^{II} complexes (M = Mo, W).[35c] $WI_2(CNDipp)_5$ also exhibited a broad, intense ν(CN) stretch centered at 2050 cm^{-1}, intermediate between that of uncomplexed CNDipp (2114 cm^{-1}) and $W(CNDipp)_6$ (1938 cm^{-1}), consistent with attenuated π-back-donation from the W^{II} center. Although $WI_2(CNDipp)_5$ absorbs fairly strongly in the region 300–500 nm ($\varepsilon_{\lambda,max} \sim 10^4$ M^{-1} cm^{-1}, Figures S24–S28), the complex did not luminesce when excited at 445 nm, as expected from the observed loss of $W(CNAr)_6$ luminescence during photoredox catalysis.

As with $W(CNDipp)_6$, photoreduction of iodobenzene by $*W(CNDippPh^{OMe3})_6$ in benzene solution formed a product (~95% isolated yield) with UV–vis and ^{1}H NMR spectroscopic signatures reminiscent of those observed in the corresponding post-photoredox catalysis reaction mixtures. Despite numerous attempts, single crystals of the product suitable for XRD analysis could not be grown. However, because it shares similar ^{1}H/^{13}C NMR, UV–vis, IR, and CV data with $WI_2(CNDipp)_5$, we suggest that this new complex is $WI_2(CNDippPh^{OMe3})_5$ (Scheme 1).

CVs of $WI_2(CNDipp)_5$ displayed quasi-reversible oxidation and irreversible reduction waves at –0.07 and –2.31 V vs $Fc^{[+/0]}$, respectively (Figure 6), with relative integration revealing that twice the amount of charge was passed in the latter. We therefore assign these as 1-electron $W^{[3+/2+]}$ and 2-electron $W^{[2+/0]}$ redox events. In this regard, the electrochemical behavior mirrors that of related $[M(CNPh)_7]^{2+}$ (M = Mo, W) and $[MoI(CNPh)_6]^+$ complexes.[19,22,38] Of interest is that oxidation and reduction of $WI_2(CNDipp)_5$ occurred at more negative potentials, in line with replacement of uncharged π-accepting arylisocyanides by anionic iodide ligands to yield an overall neutral complex. Extrapolation of $[M(CNPh)_7]^{2+}$ and $[MoI(CNPh)_6]^+$ formal potentials also indicated that $E°$ ($W^{[3+/2+]}$) and $E_{p,c}°$ ($W^{[2+/0]}$) will be similar to those experimentally determined for $WI_2(CNDipp)_5$ (Supporting Information, Table S6).

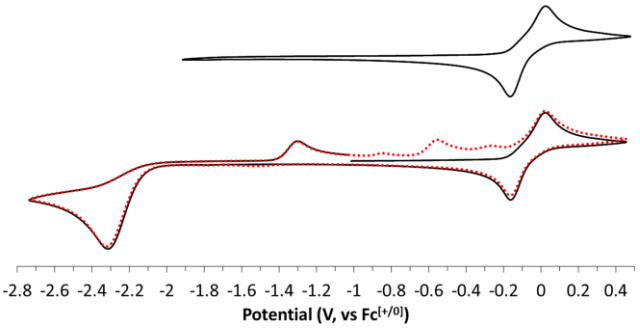

Figure 6. Cyclic voltammograms of $WI_2(CNDipp)_5$ at a scan rate of 100 mV s^{-1} in THF with 0.1 M [^{n}Bu$_4$N][PF_6] supporting electrolyte (vs $Fc^{[+/0]}$). Cycles 1 and 2 (lower CVs) are depicted as solid black and dotted red traces, respectively.

Scanning cathodically from the $WI_2(CNDipp)_5$ $W^{[2+/0]}$ feature produced oxidation waves in the return scan that could not be reliably assigned (Figure 6, bottom). At more negative potentials, an irreversible cathodic event at –3.3 V (vs $Fc^{[+/0]}$) attributable to CNDipp-based reduction was observed (Figure S145). The CVs of $WI_2(CNDippPh^{OMe3})_5$ are analogous to those of $WI_2(CNDipp)_5$, displaying quasi-reversible $W^{[3+/2+]}$ and irreversible $W^{[2+/0]}$ features at –0.06 and –2.35 V, respectively (Figure S148).

Attempts to regenerate $W(CNDipp)_6$ from $WI_2(CNDipp)_5$ electrochemically were unsuccessful,[39] as CVs of $WI_2(CNDipp)_5$ collected in the presence of excess CNDipp (up to 51 equiv) did not reveal a well-defined $W(CNDipp)_6^{[+/0]}$ wave upon scanning cathodically of the irreversible $W^{[2+/0]}$ couple. However, Na(Hg) reduction of $WI_2(CNDipp)_5$, followed by addition of CNDipp, regenerated $W(CNDipp)_6$ (supported by UV–vis and ^{1}H NMR data; Figures S149–S151).

In summary, $W(CNAr)_6$ complexes catalyze 1-(2-iodobenzyl)-pyrrole BHAS upon either one-photon (visible) or two-photon excitation, with the latter representing a unique approach to NIR photoredox catalysis. Our proposed photochemical model (Figure 3) suggests that the rate of catalysis is slowed by charge recombination within the solvent cage, owing to limited ion-pair separation in low dielectric solvents. Overall catalytic turnover is limited by deactivation pathways, among them the production of $WI_2(CNAr)_5$. Such pathways could be disfavored by more polar solvents or the addition of salts,[9] to promote escape of $[W(CNAr)_6]^+$ from iodide in the solvent cage. Finally, owing to exceptional TPA cross sections and excited-state reduction potentials, $W(CNAr)_6$ complexes might define an important new class of photoinitiators for 3D lithography applications.

ASSOCIATED CONTENT

Supporting Information

The Supporting Information is available free of charge at http://pubs.acs.org.

Experimental details; characterization data; spectroscopic data (^{1}H and ^{13}C NMR, IR, UV–visible absorbance, steady-state luminescence, time-resolved luminescence, and transient absorption); CVs; XRD refinement details (PDF).

Accession Codes

CCDC 2098282 contains the supplementary crystallographic data for this paper. This data can be obtained free of charge via www.ccdc.cam.ac.uk/data_request/cif, or by emailing data_request@ccdc.cam.ac.uk, or by contacting The Cambridge Crystallographic Data Centre, 12 Union Road, Cambridge CB2 1EZ, UK; fax: +44 1223 336033.

AUTHOR INFORMATION

Corresponding Authors

*email: winklerj@caltech.edu
*email: hbgray@caltech.edu

Author Contributions

All authors have given approval to the final version of the manuscript.

Funding Sources

This work was supported by the National Science Foundation (CHE-1763429) and the Caltech Beckman Institute Laser Resource Center supported by the Arnold and Mabel Beckman Foundation. The X-ray Crystallography Facility in the Beckman Institute was supported by a Dow Next Generation Instrumentation Grant.

Notes

The authors declare no competing financial interest.

ACKNOWLEDGMENTS

We thank Lawrence M. Henling for assistance with XRD experiments, and Christian M. Johansen for acquisition of IR spectra in Figure S19. We also thank Drs. Wes and Aaron Sattler for very helpful comments during preparation of this manuscript.

REFERENCES

(1) Prier, C. K.; Rankic, D. A.; MacMillan, D. W. C. Visible Light Photoredox Catalysis with Transition Metal Complexes: Applications in Organic Synthesis. *Chem. Rev.* **2013**, *113*, 5322–5363.

(2) Koike, T.; Akita, M. Visible-Light Radical Reaction Designed by Ru- and Ir-Based Photoredox Catalysis. *Inorg. Chem. Front.* **2014**, *1*, 562–576.

(3) Shaw, M. H.; Twilton, J.; MacMillan, D. W. C. Photoredox Catalysis in Organic Chemistry. *J. Org. Chem.* **2016**, *81*, 6898–6926.

(4) (a) Hernandez-Perez, A. C.; Collins, S. K. Heteroleptic Cu-Based Sensitizers in Photoredox Catalysis. *Acc. Chem. Res.* **2016**, *49*, 1557–1565. (b) Reiser, O. Shining Light on Copper: Unique Opportunities for Visible-Light-Catalyzed Atom Transfer Radical Addition Reactions and Related Processes. *Acc. Chem. Res.* **2016**, *49*, 1990–1996. (c) Larsen, C. B.; Wenger, O. S. Photoredox Catalysis with Metal Complexes Made from Earth-Abundant Elements. *Chem. – Eur. J.* **2018**, *24*, 2039–2058. (d) He, J.; Chen, C.; Fu, G. C.; Peters, J. C. Visible-Light-Induced, Copper-Catalyzed Three-Component Coupling of Alkyl Halides, Olefins, and Trifluoromethylthiolate To Generate Trifluoromethyl Thioethers. *ACS Catal.* **2018**, *8*, 11741–11748.

(5) (a) Zhang, Y.; Petersen, J. L.; Milsmann, C. A Luminescent Zirconium(IV) Complex as a Molecular Photosensitizer for Visible Light Photoredox Catalysis. *J. Am. Chem. Soc.* **2016**, *138*, 13115–13118. (b) Zhang, Y.; Lee, T. S.; Favale, J. M.; Leary, D. C.; Petersen, J. L.; Scholes, G. D.; Castellano, F. N.; Milsmann, C. Delayed Fluorescence from a Zirconium(IV) Photosensitizer with Ligand-to-Metal Charge-Transfer Excited States. *Nat. Chem.* **2020**, *12*, 345–352.

(6) Qiao, Y.; Schelter, E. J. Lanthanide Photocatalysis. *Acc. Chem. Res.* **2018**, *51*, 2926–2936.

(7) Yu, D.; To, W.-P.; Tong, G. S. M.; Wu, L.-L.; Chan, K.-T.; Du, L.; Phillips, D. L.; Liu, Y.; Che, C.-M. Luminescent Tungsten(VI) Complexes as Photocatalysts for Light-Driven C–C and C–B Bond Formation Reactions. *Chem. Sci.* **2020**, *11*, 6370–6382.

(8) Mann, K. R.; Cimolino, M.; Geoffroy, G. L.; Hammond, G. S.; Orio, A. A.; Albertin, G.; Gray, H. B. Electronic Structures and Spectra of Hexakisphenylisocyanide Complexes of Cr(0), Mo(0), W(0), Mn(I), and Mn(II). *Inorg. Chim. Acta* **1976**, *16*, 97–101.

(9) Sattler, W.; Ener, M. E.; Blakemore, J. D.; Rachford, A. A.; LaBeaume, P. J.; Thackeray, J. W.; Cameron, J. F.; Winkler, J. R.; Gray, H. B. Generation of Powerful Tungsten Reductants by Visible Light Excitation. *J. Am. Chem. Soc.* **2013**, *135*, 10614–10617.

(10) Sattler, W.; Henling, L. M.; Winkler, J. R.; Gray, H. B. Bespoke Photoreductants: Tungsten Arylisocyanides. *J. Am. Chem. Soc.* **2015**, *137*, 1198–1205.

(11) Kvapilová, H.; Sattler, W.; Sattler, A.; Sazanovich, I. V.; Clark, I. P.; Towrie, M.; Gray, H. B.; Záliš, S.; Vlček, A. Electronic Excited States of Tungsten(0) Arylisocyanides. *Inorg. Chem.* **2015**, *54*, 8518–8528.

(12) Fajardo, J.; Schwan, J.; Kramer, W. W.; Takase, M. K.; Winkler, J. R.; Gray, H. B. Third-Generation W(CNAr)$_6$ Photoreductants (CNAr = Fused-Ring and Alkynyl-Bridged Arylisocyanides). *Inorg. Chem.* **2021**, *60*, 3481–3491.

(13) Büldt, L. A.; Guo, X.; Vogel, R.; Prescimone, A.; Wenger, O. S. A Tris(Diisocyanide)Chromium(0) Complex Is a Luminescent Analog of Fe(2,2′-Bipyridine)$_3^{2+}$. *J. Am. Chem. Soc.* **2017**, *139*, 985–992.

(14) Büldt, L. A.; Guo, X.; Prescimone, A.; Wenger, O. S. A Molybdenum(0) Isocyanide Analogue of Ru(2,2′-Bipyridine)$_3^{2+}$: A Strong Reductant for Photoredox Catalysis. *Angew. Chem. Int. Ed.* **2016**, *55*, 11247–11250.

(15) Herr, P.; Glaser, F.; Büldt, L. A.; Larsen, C. B.; Wenger, O. S. Long-Lived, Strongly Emissive, and Highly Reducing Excited States in Mo(0) Complexes with Chelating Isocyanides. *J. Am. Chem. Soc.* **2019**, *141*, 14394–14402.

(16) Larsen, C. B.; Wenger, O. S. Photophysics and Photoredox Catalysis of a Homoleptic Rhenium(I) Tris(Diisocyanide) Complex. *Inorg. Chem.* **2018**, *57*, 2965–2968.

(17) Mann, K. R.; Gray, H. B.; Hammond, G. S. Excited-State Reactivity Patterns of Hexakisarylisocyano Complexes of Chromium(0), Molybdenum(0), and Tungsten(0). *J. Am. Chem. Soc.* **1977**, *99*, 306–307.

(18) Gray, H. B.; Mann, K. R.; Lewis, N. S.; Thich, J. A.; Richman, R. M. Photochemistry of Metal-Isocyanide Complexes and Its Possible Relevance to Solar Energy Conversion. In *Inorganic and Organometallic Photochemistry*; American Chemical Society, 1978; Vol. 168, 44–56.

(19) Klendworth, D. D.; Welters, W. W.; Walton, R. A. Redox Chemistry of Hexakis(Phenyl Isocyanide) Complexes of Molybdenum and Tungsten: The Synthesis of the Seven-Coordinate Cations [M(CNPh)$_7$]$^{2+}$ and Their Electrochemistry and Substitution Reactions. *Organometallics* **1982**, *1*, 336–343.

(20) Takematsu, K.; Wehlin, S. A. M.; Sattler, W.; Winkler, J. R.; Gray, H. B. Two-Photon Spectroscopy of Tungsten(0) Arylisocyanides Using Nanosecond-Pulsed Excitation. *Dalton Trans.* **2017**, *46*, 13188–13193.

(21) (a) Arnoux, C.; Konishi, T.; Van Elslande, E.; Poutougnigni, E.-A.; Mulatier, J.-C.; Khrouz, L.; Bucher, C.; Dumont, E.; Kamada, K.; Andraud, C.; Baldeck, P.; Banyasz, A.; Monnereau, C. Polymerization Photoinitiators with Near-Resonance Enhanced Two-Photon Absorption Cross-Section: Toward High-Resolution Photoresist with Improved Sensitivity. *Macromolecules* **2020**, *53*, 9264–9278. (b) Skliutas, E.; Lebedevaite, M.; Kabouraki, E.; Baldacchini, T.; Ostrauskaite, J.; Vamvakaki, M.; Farsari, M.; Juodkazis, S.; Malinauskas, M. Polymerization Mechanisms Initiated by Spatio-Temporally Confined Light. *Nanophotonics* **2021**, *10*, 1211–1242.

(22) Klendworth, D. D.; Welters, W. W.; Walton, R. A. Homoleptic Phenyl Isocyanide Complexes of Molybdenum and Tungsten: Zerovalent Six-Coordinate versus Divalent Seven-Coordinate. *J. Organomet. Chem.* **1981**, *213*, C13–C16.

(23) Performing the photoredox catalysis in the presence of increasing equivalents of TMP or excess free CNDipp did not improve the conversion or TON (Supporting Information, Figures S54–S61).

(24) Decreasing the $W(CNDipp)_6$ loading below 2.5 mol % led to further decreases in conversion, but with similar TONs (Supporting Information, Figures S62–S69).

(25) Pause, L.; Robert, M.; Savéant, J.-M. Can Single-Electron Transfer Break an Aromatic Carbon−Heteroatom Bond in One Step? A Novel Example of Transition between Stepwise and Concerted Mechanisms in the Reduction of Aromatic Iodides. *J. Am. Chem. Soc.* **1999**, *121*, 7158–7159.

(26) Robert, M.; Savéant, J.-M. Photoinduced Dissociative Electron Transfer: Is the Quantum Yield Theoretically Predicted to Equal Unity? *J. Am. Chem. Soc.* **2000**, *122*, 514–517.

(27) Edkins, R. M.; Bettington, S. L.; Goeta, A. E.; Beeby, A. Two-Photon Spectroscopy of Cyclometalated Iridium Complexes. *Dalton Trans.* **2011**, *40*, 12765–12770.

(28) Ravetz, B. D.; Tay, N. E. S.; Joe, C. L.; Sezen-Edmonds, M.; Schmidt, M. A.; Tan, Y.; Janey, J. M.; Eastgate, M. D.; Rovis, T. Development of a Platform for Near-Infrared Photoredox Catalysis. *ACS Cent. Sci.* **2020**, *6*, 2053–2059.

(29) For other examples of red-light-driven photoredox catalysis, see the following and references cited therein: Mei, L.; Gianetti, T. Helical Carbenium Ion-Based Organic Photoredox Catalyst: A Versatile and Sustainable Option in Red-Light-Induced Reactions. *Synlett* **2021**, *32*, 337–334.

(30) Ravetz, B. D.; Pun, A. B.; Churchill, E. M.; Congreve, D. N.; Rovis, T.; Campos, L. M. Photoredox Catalysis Using Infrared Light via Triplet Fusion Upconversion. *Nature* **2019**, *565*, 343–346.

(31) Bilger, J. B.; Kerzig, C.; Larsen, C. B.; Wenger, O. S. A Photorobust Mo(0) Complex Mimicking $[Os(2,2'\text{-Bipyridine})_3]^{2+}$ and Its Application in Red-to-Blue Upconversion. *J. Am. Chem. Soc.* **2021**, *143*, 1651–1663.

(32) Dewan, J. C.; Roberts, M. M.; Lippard, S. J. Geometric Isomerism in Seven-Coordinate Tungsten(II) Mixed Carbonyl-Iodide-*tert*-Butyl Isocyanide Complexes. *Inorg. Chem.* **1983**, *22*, 1529–1533.

(33) Bonati, F.; Minghetti, G. Molybdenum(II)-Isocyanide Complexes. *Inorg. Chem.* **1970**, *9*, 2642–2644.

(34) The structure of the related complex $[ReI_2(CN^tBu)_5][I_3]$ is available in the Cambridge Crystallographic Data Centre (CCDC deposition number 1993025).

(35) (a) Novotny, M.; Lippard, S. J. Heptakis(Alkyl Isocyanide)Molybdenum(II) Complexes. *J. Chem. Soc., Chem. Commun.* **1973**, *6*, 202. (b) Lewis, D. L.; Lippard, S. J. Structure of Heptakis(Tert-Butyl Isocyanide)Molybdenum(II) Hexafluorophosphate, a Seven-Coordinate Complex with C_{2v} Monocapped Trigonal Prismatic Geometry. *J. Am. Chem. Soc.* **1975**, *97*, 2697–2702. (c) Lam, C. T.; Novotny, M.; Lewis, D. L.; Lippard, S. J. Synthesis and Characterization of Seven-Coordinate Molybdenum(II) and Tungsten(II) Isocyanide Complexes. *Inorg. Chem.* **1978**, *17*, 2127–2133. (d) Brant, P.; Cotton, F. A.; Sekutowski, J. C.; Wood, T. E.; Walton, R. A. Dimolybdenum Tetraacetate and the Octachlorodimolybdate(II) Anion as Reagents for Preparing Mononuclear Molybdenum(II) Complexes: Geometry of the Hepta(Methylisocyano)Molybdenum(II) Cation. *J. Am. Chem. Soc.* **1979**, *101*, 6588–6593. (e) Szalda, D. J.; Dewan, J. C.; Lippard, S. J. Structural Studies of Three Seven-Coordinate Isocyanide Complexes of Molybdenum(II) and Tungsten(II). *Inorg. Chem.* **1981**, *20*, 3851–3857. (f) Mialki, W. S.; Wild, R. E.; Walton, R. A. Seven-Coordinate Alkyl Isocyanide and Mixed-Alkyl Isocyanide-Phosphine Complexes of Tungsten(II). *Inorg. Chem.* **1981**, *20*, 1380–1384. (g) Dewan, J. C.; Lippard, S. J. Structure of a Homoleptic Seven Coordinate Molybdenum(II) Aryl Isocyanide Complex, $[Mo(CNPh)_7](PF_6)_2$. *Inorg. Chem.* **1982**, *21*, 1682–1684. (h) Giandomenico, C. M.; Hanau, L. H.; Lippard, S. J. Improved Synthesis of Seven-Coordinate Molybdenum(II) and Tungsten(II) Isocyanide Complexes: Dealkylation of Coordinated *tert*-Butyl Isocyanide. *Organometallics* **1982**, *1*, 142–148.

(36) Lewis, D. F.; Lippard, S. J. Synthesis and Structure of Iodohexakis(*tert*-Butyl Isocyanide)Molybdenum(II) Iodide. *Inorg. Chem.* **1972**, *11*, 621–626.

(37) (a) Dreyer, E. B.; Lam, C. T.; Lippard, S. J. Synthesis and Structure of Diiododicarbonyltris(*tert*-Butyl Isocyanide)Tungsten(II), an Example of the 4:3 Piano Stool Seven-Coordinate Geometry. *Inorg. Chem.* **1979**, *18*, 1904–1908. (b) Ditri, T. B.; Moore, C. E.; Rheingold, A. L.; Figueroa, J. S. Oxidative Decarbonylation of *m*-Terphenyl Isocyanide Complexes of Molybdenum and Tungsten: Precursors to Low-Coordinate Isocyanide Complexes. *Inorg. Chem.* **2011**, *50*, 10448–10459.

(38) Caravana, Carl.; Giandomenico, C. M.; Lippard, S. J. Electrochemical Studies of Seven-Coordinated Isocyanide Complexes of Molybdenum(II) and Tungsten(II). *Inorg. Chem.* **1982**, *21*, 1860–1863.

(39) Attempts to generate $WI_2(CNDipp)_5$ (i) electrochemically from $W(CNDipp)_6$ in the presence of tetrabutylammonium iodide or (ii) chemically by treatment of $W(CNDipp)_6$ with I_2 in C_6D_6 were also unsuccessful.

For Table of Contents Only